arXiv:1403.5283v1 [cond-mat.mes-hall] 20 Mar 2014

Large conduction band and Fermi velocity spin splittings due to Coulomb interactions in single-layer MoS_2

Yago Ferreiros[1,*] and Alberto Cortijo[1,†]

[1] *Instituto de Ciencia de Materiales de Madrid, CSIC, Cantoblanco, 28049 Madrid, Spain.*

We study the effect of Coulomb interactions on the low energy band structure of single-layer transition metal dichalcogenide semiconductors using an effective low energy model. We show how a large conduction band spin splitting and a spin dependent Fermi velocity are generated in MoS_2, as a consequence of the difference between the gaps of the two spin projections induced by the spin-orbit interaction. The conduction band and Fermi velocity spin splittings found are in agreement with the optical absorption energies of the excitonic peaks A, B measured in the experiments.

PACS numbers: 31.70.-f, 73.22.-f, 78.67.-n

Introduction.— In the post-graphene era[1], the search of new low dimensional materials has placed the transition metal dichalcogenides (TMDCs) in a prominent situation. Known for decades, these materials share attracting features common to graphene: they are layered materials with strong covalent bonding within layer and weak Van der Waals interlayer forces, being perhaps the most known member the molybdenum disulphide (MoS_2)[2]. A subset of the large family of TMDCs are semiconductors, with sizable direct gaps ranging from one to several eV around the K and K' points of the Brillouin zone (BZ)[3]. The presence of a gap in the band structure is a feature that distinguish them from graphene and makes these materials highly valuable for electronic and optoelectronic applications.

Apart from their potential applicability in electronics, TMDCs monolayers are also an attractive arena research in the field of spintronics. The transition metals forming the TMDCs display a rather large intra-atomic spin-orbit interaction. Together with the absence of inversion symmetry of the crystalline structure of TMDCs monolayers, this induces a spin-splitting between the two (otherwise degenerate) spin projections in the band structure[3]. Due to time reversal symmetry requirements, this spin splitting is opposite in both valleys and consequently it allows for controlling valley population employing circularly polarized light[4].

The orbital nature of the electronic states around the K, K' points indicates that the effect of the spin-orbit interaction is quite different for the conduction band (formed predominantly by the $d_{3z^2-r^2}$ orbital, with $j_z = 0$) and the valence band (mostly made of a linear combination of the $d_{x^2-y^2}$ and d_{xy} orbitals, with $j_z = \pm 2$). Such a particular atomic band population implies that the splitting of the valence band is first order in the spin-orbit interaction, while the splitting of the conduction band is second order[5]. According to several Density Functional Theory (DFT) calculations[3, 6, 7], this favors a weak spin splitting in the conduction band, of the order of a few meV, and a considerably larger splitting in the valence band, of the order of hundreds of meV.

The experimental characterization of the low energy band structure of TMDC semiconductors is still incomplete. The most common procedure to determine the parameters entering in the band structure description, that are later employed in other methods (e. g. in tight binding calculations[8, 9]), consists in contrasting experimental data obtained by optical means with theoretical results obtained by solving the GW-corrected Kohn-Sham equations in its several variations with different degrees of success[10]. Here we follow an alternative route: we will use a self consistent GW treatment of the Coulomb interaction together with the effective Hamiltonian around the K, K' points, using experimental data and physically motivated considerations as renormalization conditions to determine the band structure parameters of the system.

The model.— We start from the following low energy bare Hamiltonian density for single-layer TMDC semiconductors close to the K, K' points[3]:

$$\begin{aligned}\mathcal{H}_0 &= \psi^+\left((\tau\sigma_x p_x + \sigma_y p_y)V_\tau^0 + \frac{\Delta^0}{2}\sigma_z s_0\right)\psi + \\ &+ \psi^+\left(\frac{\lambda_c^0}{2}\tau(\sigma_0+\sigma_z)s_z + \frac{\lambda_v^0}{2}\tau(\sigma_0-\sigma_z)s_z\right)\psi, \quad (1)\end{aligned}$$

where ($s_0 \equiv \mathbb{1}$, $s_{x,y,z}$) and ($\sigma_0 \equiv \mathbb{1}$, $\sigma_{x,y,z}$) are the Pauli and identity matrices for the spin and the sublattice degrees of freedom, respectively, $2\lambda_c^0$ ($2\lambda_v^0$) is the conduction (valence) band splitting, $\tau = \pm 1$ is the valley index, and the matrix V_τ^0 is:

$$V_{+1}^0 = \begin{pmatrix} v_+^0 & 0 \\ 0 & v_-^0 \end{pmatrix}; \quad V_{-1}^0 = \begin{pmatrix} v_-^0 & 0 \\ 0 & v_+^0 \end{pmatrix} \quad (2)$$

with $v_\pm^0$ the Fermi velocities for spin up/down $(+/-)$ electrons. The superscript 0 is the notation used for the bare parameters. Although the Fermi velocities for both spins are assumed to be equal in the absence of interactions (since the hopping parameters should be insensitive to spin), we define the bare Fermi velocity for each spin separately, because as we will see, quantum corrections renormalize each velocity differently.

Coulomb interaction will be modeled by a coupling to an auxiliary scalar field φ[11]:

$$\mathcal{H}_{int} = e\psi^\dagger\psi\varphi + \epsilon\varphi|\vec{\nabla}|\varphi, \tag{3}$$

where ϵ is the dielectric permitivity (we use units $\hbar = 1$ at the intermediate stages, restoring standard units at the end of the calculations).

Schwinger-Dyson equations.— To self-consistently find the effects of the interaction on the low energy band structure we shall make use of the Schwinger-Dyson equation for the electron propagator[12–14]:

$$\Sigma_\tau(p) = e^2 \int \frac{d^3q}{(2\pi)^3} D(q) G_\tau(p-q), \tag{4}$$

where $D(q)^{-1} = \epsilon|\vec{q}| + \Pi(q)$ is the (inverse of the) dynamically screened Coulomb interaction (with $\Pi(q)$ the dressed polarization function) and $G_\tau(p)^{-1} = G_0^{-1}(p) + \Sigma_\tau(p)$ is the (inverse of the) full fermion propagator. The form of the self-energy $\Sigma_\tau(p)$ can be parametrized in terms of corrections to the bare parameters defined in Eq.(1):

$$\begin{aligned}\Sigma_\tau(p) &= -(\tau\sigma_x p_x + \sigma_y p_y)\delta V_\tau - \frac{\delta\Delta}{2}\sigma_z s_0 - \\ &- \frac{\delta\lambda_c}{2}\tau(\sigma_0+\sigma_z)s_z - \frac{\delta\lambda_v}{2}\tau(\sigma_0-\sigma_z)s_z. \end{aligned}\tag{5}$$

The renormalized parameters are defined as the sum of the bare parameters plus the quantum corrections:

$$\Delta = \Delta^0 + \delta\Delta, \quad \lambda_{c,v} = \lambda^0_{c,v} + \delta\lambda_{c,v}, \quad v_\pm = v^0_\pm + \delta v_\pm. \tag{6}$$

The computation of $\Pi(q)$ to leading order in a $1/N$ expansion, where N is the number of fermion flavors ($N = 2$ in our case, one for each valley), is a standard calculation and the result reads[14, 15]:

$$\Pi(q) = \frac{e^2}{4\pi}|\vec{q}|^2 \sum_{s=\pm}\left[\frac{2m_s}{q_s^2} + \frac{q_s^2 - 4m_s^2}{q_s^3}\arctan\left(\frac{q_s}{2m_s}\right)\right], \tag{7}$$

where $s = \pm$ denotes the spin degrees of freedom, $q_s^2 = q_0^2 + v_s^2|\vec{q}|^2$, $m_+ = (\Delta + \lambda_c - \lambda_v)/2$ and $m_- = (\Delta - \lambda_c + \lambda_v)/2$.

From now on we will work with only one of the two valleys: $\tau = +1$, since it can be easily seen that the equations obtained for one valley are going to be equivalent to those obtained for the other valley. The next step is to compute:

$$e^2 \int \frac{d^3q}{(2\pi)^3} D(q) G_{+1}(p-q) \equiv \begin{pmatrix} I_+(p) & 0 \\ 0 & I_-(p)\end{pmatrix}, \tag{8}$$

with:

$$I_s(p) = -I_s^z\sigma_z - v_s I_s(\sigma_x p_x + \sigma_y p_y) + \mathcal{O}(p^2) \tag{9}$$

Performing the integral in Eq.(8) we obtain[27]:

$$I_s^z = \frac{3m_r}{4}\ln\left(1 + \frac{2g_s m_s}{3m_r}\right) + \frac{g_s m_s}{2+\pi g_r}\ln\left(\frac{\Lambda v_s}{m_s}\right), \tag{10a}$$

$$I_s = \frac{3m_r}{4m_s}\ln\left(1 + \frac{2g_s m_s}{3m_r}\right) + \frac{g_s}{4+2\pi g_r}\ln\left(\frac{\Lambda v_s}{m_s}\right), \tag{10b}$$

where Λ is a momentum cut-off and we have defined:

$$g_s = e^2/(4\pi\epsilon v_s); \quad g_r = e^2/(4\pi\epsilon v_r),$$

$$m_r = \frac{2\,m_+ m_-}{m_+ + m_-}; \quad v_r = \frac{2\,v_+ v_-}{v_+ + v_-}. \tag{11}$$

In terms of the quantities $I_s^z(p)$, and $I_s(p)$, the Schwinger-Dyson equations are written as:

$$\Sigma(p) = \begin{pmatrix} I_+(p) & 0 \\ 0 & I_-(p)\end{pmatrix}. \tag{12}$$

Eq. (12) is a set of four equations for the diagonal elements (two for each spin), from which only three are linearly independent, and four equations for the off-diagonal elements, from which only two (one for each spin) are linearly independent. Thus we have five linearly independent equations for five variables:

$$\begin{aligned}\frac{\delta\Delta}{2} + s\delta\lambda_c = -I_s^z \quad , \quad \frac{\delta\Delta}{2} - \delta\lambda_v = -I_+^z, \\ -\delta v_s \;=\; v_s I_s. \end{aligned}\tag{13}$$

From these equations we can obtain the quantum corrections $\delta\Delta, \delta\lambda_{c,v}, \delta v_\pm$ as functions of the bare parameters $\Delta^0, \lambda^0_{c,v}, v^0_\pm$, and the cut-off Λ.

Renormalization: matching the experimental data— To eliminate the dependence of the quantum corrections on the bare parameters and the cut-off one needs to impose renormalization conditions, which should be obtained from experiments. In the case of single layer TMDC semiconductors the most relevant data are the energies of two excitonic peaks A, B found in absorbance experiments in MoS_2[2, 4, 16, 17], which provide two renormalization conditions.

We will focus our attention on MoS_2, as this is the most studied compound of the family of TMDCs, both theoretically and experimentally. For MoS_2 on a quartz substrate, the excitonic peaks A, B found in absorbance experiments are centered at energies of $E_A = 1.85$ eV and $E_B = 1.98$ eV[16]. The absorption energy difference between these two peaks is a direct consequence of the splitting of the spin up and spin down bands. *Ab initio* calculations give a very small conduction band splitting of approximately $2|\lambda_c| \sim 3$ meV [6, 7, 10, 18–21]. Hence, according to first principles-based calculations, the difference between the optical absorption energies of the

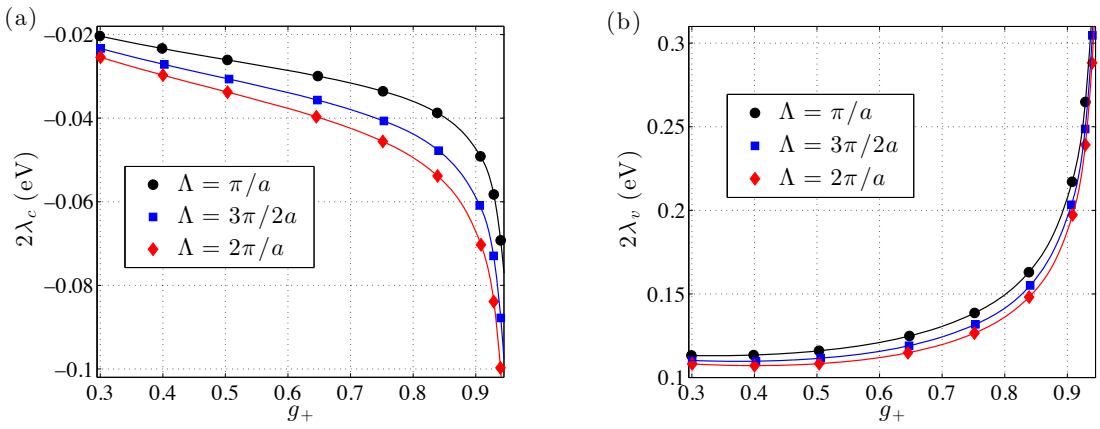

FIG. 1: Values for the $\tau = +1$ valley of the absolute value of conduction band splitting (a) and valence band splitting (b) as a function of the corrected coupling constant for spin up electrons g_+, for three different values of the momentum cut-off (in units of $\hbar$).

peaks A and B is related almost entirely to a large value of the valence band splitting[10, 20, 21]. Even analytical calculations of the excitonic properties of MoS_2 use as an input the parameter values obtained by *ab initio* calculations[22].

The optical absorption energies of the excitonic bound states are obtained by solving the two particle problem for the Dirac equation. The expressions for the energies of the lowest excitonic states are[23]:

$$E_{A,B} = E_\pm = m_\pm \left(1 + \sqrt{1 - g_\pm^2}\right). \qquad (14)$$

These are the two experimental conditions that have to be fulfilled by the renormalized parameters $\Delta, \lambda_{c,v}, v_\pm$. The dielectric permittivity ϵ that enters in the coupling constant $g_\pm$ can be written as $\epsilon = \epsilon_0(\epsilon_s + \epsilon_m)/2$, being ϵ_0 the dielectric permittivity of the vacuum and $\epsilon_{s,m}$ the dielectric constants of the substrate and material (MoS_2) respectively. As we are working on a quartz substrate, we have $\epsilon_s = 3.9$, while for the dielectric constant of MoS_2 we use $\epsilon_m = 3.4$[20]. Notice that Eq.(14) assumes equal hole and electron effective masses.

As we said, the energies in Eq. (14) are obtained by solving the two particle problem[16]. This is a sensible approach since we are working in the instantaneous approximation, so the self consistent solution of the Schwinger-Dyson equations provides no term proportional to the frequency p_0 in Eq.(9). This implies that there is no wave function renormalization Z_ψ, and there is no loss of electronic coherence. This fact, together with the absence of any imaginary part in $\Sigma_\tau(p)$, means that the poles in the full two-particle propagator will coincide with the ones in the non interacting two particle propagator, but dressed with the renormalized parameters in the Green functions[24]

Since the excitonic data are not enough to fully execute the renormalization program, we are going to impose two additional conditions so that the renormalized parameters will depend only on one bare parameter and the cut-off. At very small interactions (at very high dielectric permittivity $\epsilon \to \infty$), we will force a zero conduction band splitting $\lambda_c = 0$ and equal Fermi velocities for both spin projections $v_+ = v_-$. The motivation for this choice comes from the fact that for $\epsilon \to \infty$ quantum corrections are negligible (assuming a finite physical cut-off), and the conduction band should remain (approximately) degenerate in spin due to the nature of the wave functions[5], while the hopping parameters should be insensitive to spin. In this limit the conditions on the renormalized parameters translate to conditions on the bare parameters: $\lambda_c^0 = 0$ and $v_+^0 = v_-^0$.

Since we have imposed two extra conditions, we still have two free parameters: v_+^0 and the momentum cut-off Λ. We then solve the Schwinger-Dyson equations for different values of the cut-off and the Fermi velocity bare parameter, and give the results as a function of the renormalized coupling constant g_+.

Solution of the Schwinger-Dyson equations.— We will present the results for one of the two valleys ($\tau = +1$). The values for the other valley are obtained by changing the sign of $\lambda_{c,v}$, and consequently interchanging the values of the masses ($m_+ \leftrightarrow m_-$) and the Fermi velocities ($v_+ \leftrightarrow v_-$).

In Figs.1,2 the values of different renormalized parameters as functions of g_+ are plotted for three different values of Λ. From Figs.1(a,b) we see that the Coulomb interaction enlarges both the value of the valence band splitting and the (absolute) value of the conduction band splitting. Let us remember that all the plotted values are constrained to match the experimental energies of the excitonic peaks E_A and E_B. As an example, for a coupling constant $g_+ = 0.93$ and a physical momentum cut-off $\Lambda = 2\hbar\pi/a$ (the lattice constant is taken to be $a = 3.193$ Å[3]), we have an scenario with a conduction band split-

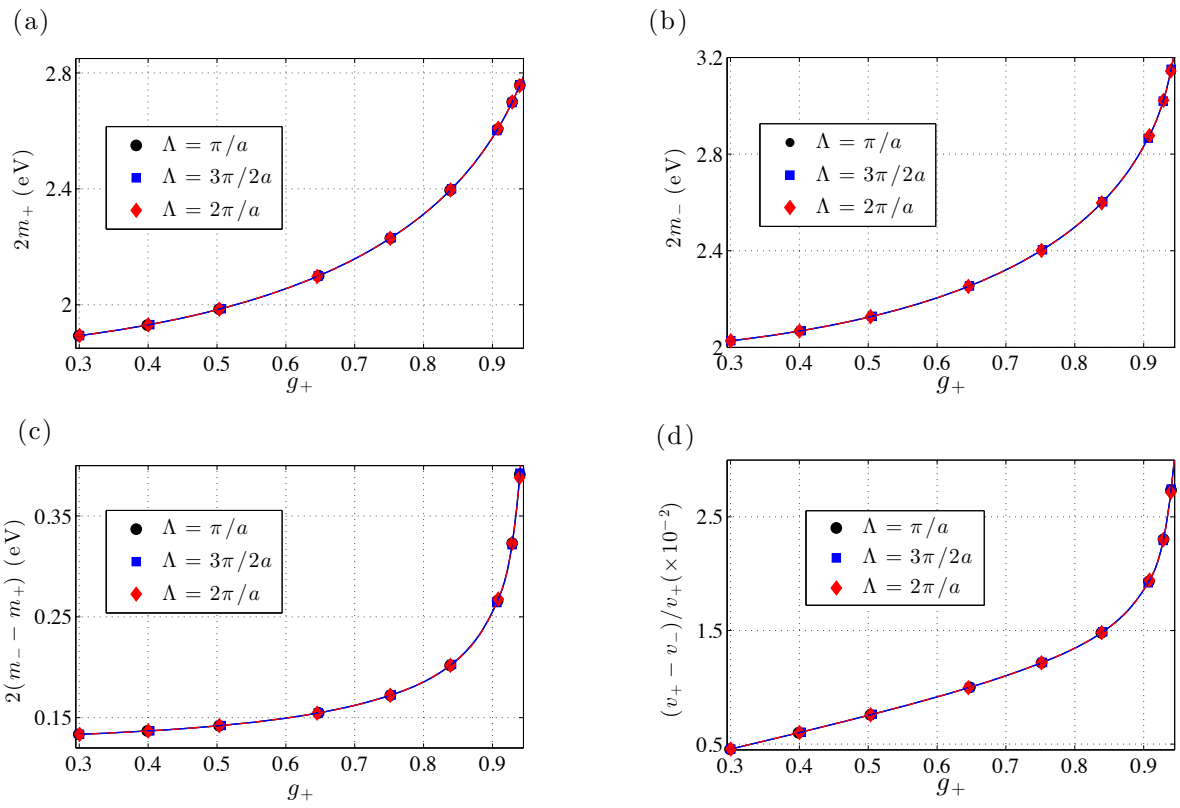

FIG. 2: Values for the $\tau = +1$ valley of the gap for the spin up electrons (a), gap for the spin down electrons (b), gap difference between spin down and up electrons (c) and normalized Fermi velocity difference between spin up and down electrons (d), as a function of the corrected coupling constant for spin up electrons g_+, for three different values of the momentum cut-off (in units of $\hbar$).

ting $2|\lambda_c| = 70$ meV, fully compatible with the measured optical absorption energies of the excitonic peaks A, B.

Also from Fig.1(a,b) we can see that the (absolute) value of the conduction band splitting increases with increasing cut-off Λ, while the contrary is found for the valence band splitting. This might seem counter-intuitive at a first sight, but it is a result of the renormalization conditions imposed.

We restricted ourselves to values of the coupling constant in the region $g_\pm < 1$. The reason for this is that the validity of Eq.(14) no longer holds for $g_\pm \geq 1$, as the lowest excitonic energies would become imaginary. For such values of g_+, an ultraviolet regularization is needed to deal with the singularity of the Coulomb potential[23, 25, 26], and imposing the experimental conditions for the excitonic peaks becomes more involved. However, this is not a technical caveat for the renormalization scheme, and the present calculations could be extended to this region with the corresponding computational effort.

The behavior for big values of g_+ of the difference between spin down and up gaps $2(m_- - m_+)$ plotted in Fig. 2(c), as well as the valence and conduction band splittings (Figs. 1(a,b)), is influenced by the splitting of the Fermi velocities induced by the quantum corrections (Fig. 2(d)). It can be seen from eqs.(14) that the greater this splitting is, the greater the difference $m_- - m_+$ becomes. This influences also the values of $\lambda_{c,v}$, as $m_- - m_+ = \lambda_v - \lambda_c$. We actually find values for $m_- - m_+$ considerably larger than those reported in previous (*ab initio*) calculations[10, 20, 21], as a consequence of the splitting of the Fermi velocity.

We also point out that both the difference between spin up and down Fermi velocities and the gaps are cut-off independent. For the Fermi velocity difference, the independence on the cut-off Λ can be derived from eqs. (10b,13). The correction to the Fermi velocity is given by $\delta v_s = v_s I_s$, and if we do $\delta v_+ - \delta v_-$, the two logarithms which give the explicit dependence on Λ are subtracted, so the explicit dependence vanishes. There is however an implicit dependence on Λ coming from v_s and m_s. From conditions (14) we obtain m_s as a function of v_s, so all the implicit dependence on the cut-off lies in v_s. With the extra condition $v_+^0 = v_-^0$, we can write $v_- = v_+ - \delta v_+ + \delta v_-$, and for any given v_+ we have an equation for $\delta v_+ - \delta v_-$ independent of Λ. With the Fermi velocity

difference being cut-off independent, from conditions (14) one automatically obtains cut-off independent masses for each spin.

Summary.— Large conduction band and Fermi velocity spin splittings are found due to the effect of Coulomb interactions, fully consistent with optical absorption measurements. The ultimate reason of these splittings is the presence of a different gap for the two spin polarization species, which induces a different renormalization of the gap and Fermi velocities of the two spin projections. To ensure consistency with absorption experiments, we used the values of the measured energies of the excitonic peaks of MoS_2 on a quartz substrate as renormalization conditions.

Acknowledgments.—A. C. gratefully acknowledges conversations with M. A. H. Vozmediano and R. Asgari at the early stages of this project, and with E. Cappelluti. This research is partially supported by CSIC JAEdoc fellowship program and the Spanish MECD Grants No. FIS2011-23713 and No. PIB2010BZ-00512.

* Electronic address: yago.ferreiros@csic.es
† Electronic address: alberto.cortijo@csic.es

[1] A. H. Castro Neto, F. Guinea, N. M. R. Peres, K. S. Novoselov, and A. K. Geim, Rev. Mod. Phys. **81**, 109 (2009).
[2] K. F. Mak, C. Lee, J. Hone, J. Shan, and T. F. Heinz, Phys. Rev. Lett. **105**, 136805 (2010).
[3] D. Xiao, G.-B. Liu, W. Feng, X. Xu, and W. Yao, Phys. Rev. Lett. **108**, 196802 (2012).
[4] K. F. Mak, K. He, J. Shan, and T. F. Heinz, Nature Nanotechnology **7**, 494 (2012).
[5] H. Ochoa and R. Roldán, Phys. Rev. B **87**, 245421 (2013).
[6] K. Kośmider, J. W. González, and J. Fernández-Rossier, Phys. Rev. B **88**, 245436 (2013).
[7] A. Kormányos, V. Zólyomi, N. D. Drummond, P. Rakyta, G. Burkard, and V. I. Fal'ko, Phys. Rev. B **88**, 045416 (2013).
[8] E. Cappelluti, R. Roldán, J. A. Silva-Guillén, P. Ordejón, and F. Guinea, Phys. Rev. B **88**, 075409 (2013).
[9] H. Rostami, A. G. Moghaddam, and R. Asgari, Phys. Rev. B **88**, 085440 (2013).
[10] D. Y. Qiu, F. H. da Jornada, and S. G. Louie, Phys. Rev. Lett. **111**, 216805 (2013).
[11] J. González, F. Guinea, and M. A. H. Vozmediano, Phys. Rev. B **59**, R2474 (1999).
[12] F. J. Dyson, Phys. Rev. **75**, 1736 (1949).
[13] J. Schwinger, PNAS **37**, 452 (1951).
[14] T. W. Appelquist, M. Bowick, D. Karabali, and L. C. R. Wijewardhana, Phys. Rev. D **33**, 3704 (1986).
[15] F. S. Nogueira and I. Eremin, Phys. Rev. B **88**, 085126 (2013).
[16] A. Splendiani, L. Sun, Y. Zhang, T. Li, J. Kim, C.-Y. Chim, G. Galli, and F. Wang, Nano Lett. **10**, 1271 (2010).
[17] K. F. Mak, K. He, C. Lee, G. H. Lee, J. Hone, T. F. Heinz, and J. Shan, Nature Materials **12**, 207 (2013).
[18] E. S. Kadantsev and P. Hawrylak, Solid State Communications **152**, 909 (2012), ISSN 0038-1098.
[19] K. Kośmider and J. Fernández-Rossier, Phys. Rev. B **87**, 075451 (2013).
[20] T. Cheiwchanchamnangij and W. R. L. Lambrecht, Phys. Rev. B **85**, 205302 (2012).
[21] A. Molina-Sánchez, D. Sangalli, K. Hummer, A. Marini, and L. Wirtz, Phys. Rev. B **88**, 045412 (2013).
[22] G. Berghäuser and E. Malic, ArXiv e-prints (2013), 1311.1045.
[23] A. S. Rodin and A. H. Castro Neto, Phys. Rev. B **88**, 195437 (2013), 1305.4278.
[24] O. V. Gamayun, E. V. Gorbar, and V. P. Gusynin, Phys. Rev. B **80**, 165429 (2009).
[25] D. S. Novikov, Phys. Rev. B **76**, 245435 (2007).
[26] V. M. Pereira, V. N. Kotov, and A. H. Castro Neto, Phys. Rev. B **78**, 085101 (2008).
[27] See Supplemental Material at (...) for details on the computation of the fermionic self-energy.

SUPPLEMENTAL MATERIAL: EFFECT OF COULOMB INTERACTIONS ON THE LOW ENERGY BAND STRUCTURE OF SINGLE-LAYER MOS_2

Computation of the fermionic self-energy

The fermionic self-energy is given by the Schwinger-Dyson equation for the fermionic propagator:

$$\Sigma_\tau(p) = e^2 \int \frac{d^3q}{(2\pi)^3} D(q) G_\tau(p-q), \tag{15}$$

where Σ_τ is the self-energy for each valley $\tau = \pm 1$, and D and $G_\tau = (G_0^{-1} + \Sigma_\tau)^{-1}$ are the auxiliary scalar field and full fermionic propagators respectively:

$$D^{-1}(q) = \epsilon|\vec{q}| + \Pi(q), \tag{16}$$

and

$$\Sigma_\tau(p) = -(\tau\sigma_x p_x + \sigma_y p_y)\delta V_\tau - \frac{\delta\Delta}{2}\sigma_z s_0 - \\ -\frac{\delta\lambda_c}{2}\tau(\sigma_0+\sigma_z)s_z - \frac{\delta\lambda_v}{2}\tau(\sigma_0-\sigma_z)s_z. \tag{17}$$

Notice that we are working in imaginary time. The renormalized parameters are defined as the sum of the bare parameters, denoted by the super index (0), plus the quantum corrections:

$$\Delta = \Delta^0 + \delta\Delta, \qquad \lambda_{c,v} = \lambda^0_{c,v} + \delta\lambda_{c,v}, \\ v_\pm = v^0_\pm + \delta v_\pm. \tag{18}$$

$\Pi(q)$ is the scalar field self-energy, which dresses the Coulomb interaction, given by (at leading order in a $1/N$ expansion):

$$\Pi(q) = \frac{e^2}{4\pi}|\vec{q}|^2 \sum_{s=\pm}\left[\frac{2m_s}{q_s^2} + \frac{q_s^2 - 4m_s^2}{q_s^3}\arctan\left(\frac{q_s}{2m_s}\right)\right] \tag{19}$$

where $s = \pm$ denotes the spin degrees of freedom, $q_s^2 = q_0^2 + v_s^2|\vec{q}|^2$, $m_+ = (\Delta + \lambda_c - \lambda_v)/2$ and $m_- = (\Delta - \lambda_c + \lambda_v)/2$. We will work in the instantaneous approximation $q_0 = 0$. We shall need to know the asymptotic behavior of $\Pi(q)$ in the limits of low and high momenta. For $v_s|\vec{q}| << m_s$ we have:

$$\Pi(|\vec{q}|) = \frac{e^2}{3\pi m_r}|\vec{q}|^2, \tag{20}$$

with

$$m_r = \frac{2\,m_+ m_-}{m_+ + m_-}. \tag{21}$$

In the opposite limit, $v_s|\vec{q}| >> m_s$:

$$\Pi(|\vec{q}|) = \frac{e^2}{4v_r}|\vec{q}| \tag{22}$$

with:

$$v_r = \frac{2\,v_+ v_-}{v_+ + v_-}. \tag{23}$$

From now on we will work with only one of the two valleys, namely $\tau = +1$. To obtain the self-energy we need to compute the integral:

$$\Sigma(p) \equiv \begin{pmatrix} I_+(p) & 0 \\ 0 & I_-(p)\end{pmatrix} = e^2\int\frac{d^3q}{(2\pi)^3}D(q)G_{+1}(p-q), \tag{24}$$

with, keeping terms up to first order in p:

$$I_s(p) = -\begin{pmatrix} I_s^{(1)} & 0 \\ 0 & I_s^{(2)}\end{pmatrix} - v_s I_s(\sigma_x p_x + \sigma_y p_y). \tag{25}$$

From the low energy Hamiltonian given in the main text one extracts the inverse bare fermion propagator. Inverting it and replacing the bare parameters by the renormalized ones, we get the full fermion propagator which enters the integral. Inserting the explicit values of $D(q)$ and $G_{+1}(p-q)$ we have:

$$I_s^{(j)} = i2\pi g_s\left(\int_0^{m_s}\frac{d|\vec{q}|}{2\pi}\left(1+\frac{4g_s}{6m_r}|\vec{q}|\right)^{-1} + (1+\pi g_r/2)^{-1}\int_{m_s}^{\Lambda v_s}\frac{d|\vec{q}|}{2\pi}\right)\times \\ \times \int_{-\infty}^{\infty}\frac{dq_0}{2\pi}g_0^s(q)\left(q_0 + i(-1)^j\frac{\Delta}{2} + s\,i\Big((j-1)\lambda_c + (2-j)\lambda_v\Big)\right), \tag{26}$$

$$I_s = 2\pi g_s\left(\int_0^{m_s}\frac{d|\vec{q}|}{2\pi}\left(1+\frac{4g_s}{6m_r}|\vec{q}|\right)^{-1} + (1+\pi g_r/2)^{-1}\int_{m_s}^{\Lambda v_s}\frac{d|\vec{q}|}{2\pi}\right)\int_{-\infty}^{\infty}\frac{dq_0}{2\pi}g_0^s(q)\left(1-|\vec{q}|^2 g_0^s(q)\right), \tag{27}$$

with $g_s = e^2/(4\pi\epsilon v_s)$, $g_r = e^2/(4\pi\epsilon v_r)$ and

$$g_0^s(q) = \left(\Big(q_0 + s\,\frac{i}{2}(\lambda_c+\lambda_v)\Big)^2 + |\vec{q}|^2 + m_s^2\right)^{-1}. \tag{28}$$

Note that we divided the momentum integral in two re-

gions, one for $v_s|\vec{q}| << m_s$ and another for $v_s|\vec{q}| >> m_s$, using the expansions of eqs. (20) and (22). Note also that we introduced a momentum cut-off Λ, as the momentum integrals diverge. When doing the integrals in q_0 one should be careful and expand the results in $|\vec{q}|$ accordingly for each momentum integral region $v_s|\vec{q}| << m_s$ and $v_s|\vec{q}| >> m_s$. Doing the integrals we finally arrive to:

$$I_s^{(j)} = (-1)^{j+1} I_s^z, \tag{29a}$$

$$I_s^z = \frac{3m_r}{4} \ln\left(1 + \frac{2g_s m_s}{3m_r}\right) + \frac{g_s m_s}{2 + \pi g_r} \ln\left(\frac{\Lambda v_s}{m_s}\right), \tag{29b}$$

$$I_s = \frac{3m_r}{4m_s} \ln\left(1 + \frac{2g_s m_s}{3m_r}\right) + \frac{g_s}{4 + 2\pi g_r} \ln\left(\frac{\Lambda v_s}{m_s}\right), \tag{29c}$$

which are the expressions used in the main text.